NRIAG JOURNAL OF ASTRONOMY AND GEOPHYSICS
2020, VOL. 9, NO. 1, 393–401
https://doi.org/10.1080/20909977.2020.1743019

Application of 3D Euler Deconvolution and 2D inverse modelling to basin depth estimation, the case of the Keta basin, Ghana

Nuamah Daniel O. B.[a] and Tandoh Kingsley K.[b]

[a]Department of Geophysics, University of Miskolc, Miskolc, Hungary; [b]Department of Oil and Gas Engineering, All Nations University College, Koforidua, Ghana

ABSTRACT

3D Located Euler Deconvolution and 2D Inverse Modelling have been applied to aero-magnetic and gravity data, respectively, to estimate depth to the basement across the Keta-basin, South-eastern Ghana, West Africa. The Euler deconvolution estimated relative depths, illustrated by depth solutions across the entire basin while the inverse modelling estimated the absolute depth at various positions in the basin. To improve and provide more accurate depth solutions, we applied the Located 3D Euler Deconvolution Method instead of the Standard Euler Deconvolution. The Located Euler depth estimate were obtained by calculating an analytic signal grid, finding peaks in the grid, then using the peak locations for located 3D Euler deconvolution. This method produced far lesser solutions than the Standard 3D Euler deconvolution. To estimate absolute depths across the basin, 2D inverse models were created along with five profiles constructed across strike on the gravity bouguer anomaly map. An Iterative Least Squares Inversion Method which is a non-linear inversion technique was applied to automatically calculate the model parameter (depths) in each step of the iteration process. The inversion procedure can easily be integrated with geologically realistic models. Comparatively, both methods produced similar depth estimates. The study showed higher depths to the south and east of the study area (>2 km) as the shallower depth occurs to the north (<2 km). The relative thickness of sedimentary succession was inferred from the depth distribution patterns as observed from Euler depth solutions. The highest depth estimated was 3.57 km which occur further south of the basin.

ARTICLE HISTORY
Received 2 March 2019
Revised 12 February 2020
Accepted 10 March 2020

KEYWORDS
Euler Deconvolution; inverse Modelling; depth Measurements; Bouguer anomaly

1. Introduction

The Keta basin (Figure 1) is located at the south-eastern part of Ghana and covers approximately 2,200 sq.km in a region dominated by the Volta river delta complexes (Akpati 1975). It is one of the chains of Mesozoic and Tertiary sedimentary basins in the Gulf of Guinea (Atta-Peters et al. 2012). The basin is bounded by latitudes 5◦44′44” N and 6◦33′37” N and longitudes 00◦35′10” W and 1◦’10′10” E. In terms of physiography, the keta coastal basin is relatively flat and low-lying, with elevations ranging from sea level up to approximately 150 m. The basins boundary follows the Ghana and Togo political boundary to the northeast and the coastline to the south. The off-shore Keta basin has seen extensive oil and gas exploration over the years with a recent discovery and production of gas in commercial quantities. This study tries to evaluate depth to the basement onshore and across the immediate shelf using 3D Euler Deconvolution and 2D Inverse Modelling.

Depth to basement estimation is an important practice in oil and gas exploration. Several methods have been developed over the years to maximise its estimation accuracies which include the 3D Euler Deconvolution and Geophysical Inversion Techniques. This study was conducted on the Keta basin to assess the effectiveness of these methods and provide comparative analyses of their result. Depth measurements are important because they present a fair idea about the thickness of sedimentary succession and are used in establishing drilling parameters. They are also incorporated into various models in the exploration process. The objective of the located 3D Euler deconvolution process was to produce a map showing the locations and corresponding depth estimations of geologic sources of magnetic anomalies in a two-dimensional grid (Reid et al. 1990). Hence, enabling relative depth estimation across the basin. The 2D inversion, on the other hand, was applied to estimate the absolute depth at distinct locations.

1.1. Regional tectonic setting

The Keta basin forms part of the Gulf of Guinea Province which includes the Ivory Coast, Tano, Saltpond, Central, Keta, and Benin Basins as well as the Dahomey Embayment in the northwestern part of the Gulf of Guinea (Figure 2). These basins share common structural and stratigraphic characteristics, in that they are wrench-modified basins (Clifford 1986) and contain rocks ranging in age from Ordovician to Holocene (Kjemperud et al.

CONTACT Tandoh Kingsley K. Oil and Gas Engineering Department, All Nations University College, P. O. Box KF 1908, Koforidua, Ghana

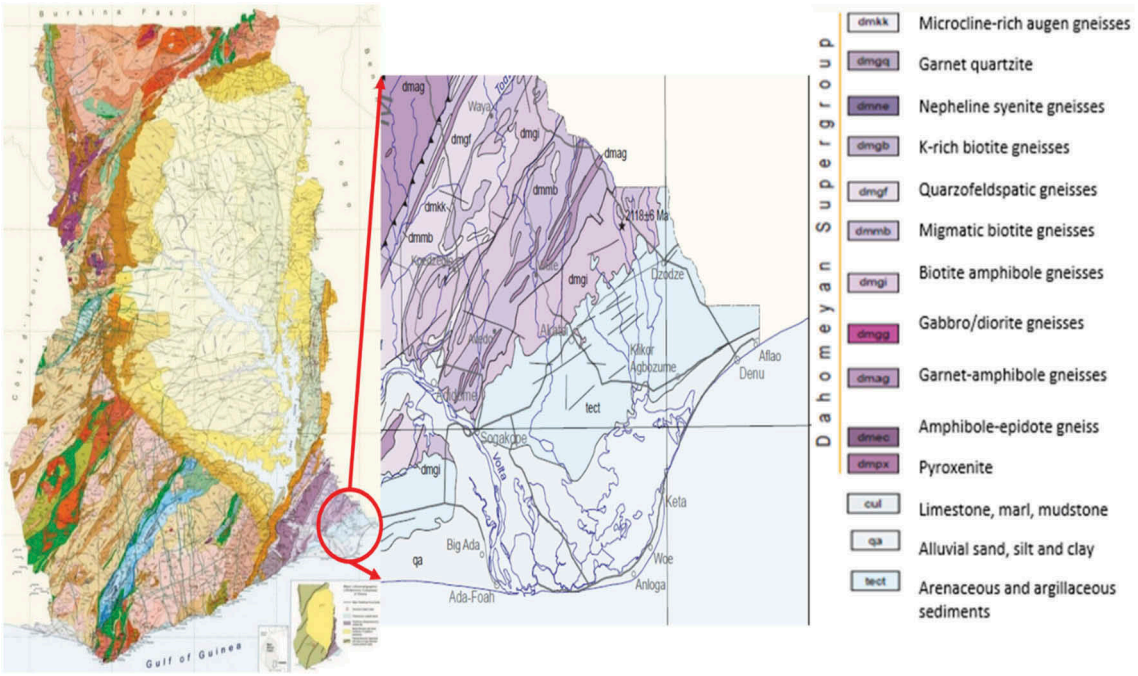

Figure 1. Map of Ghana showing the location and size of the study area.

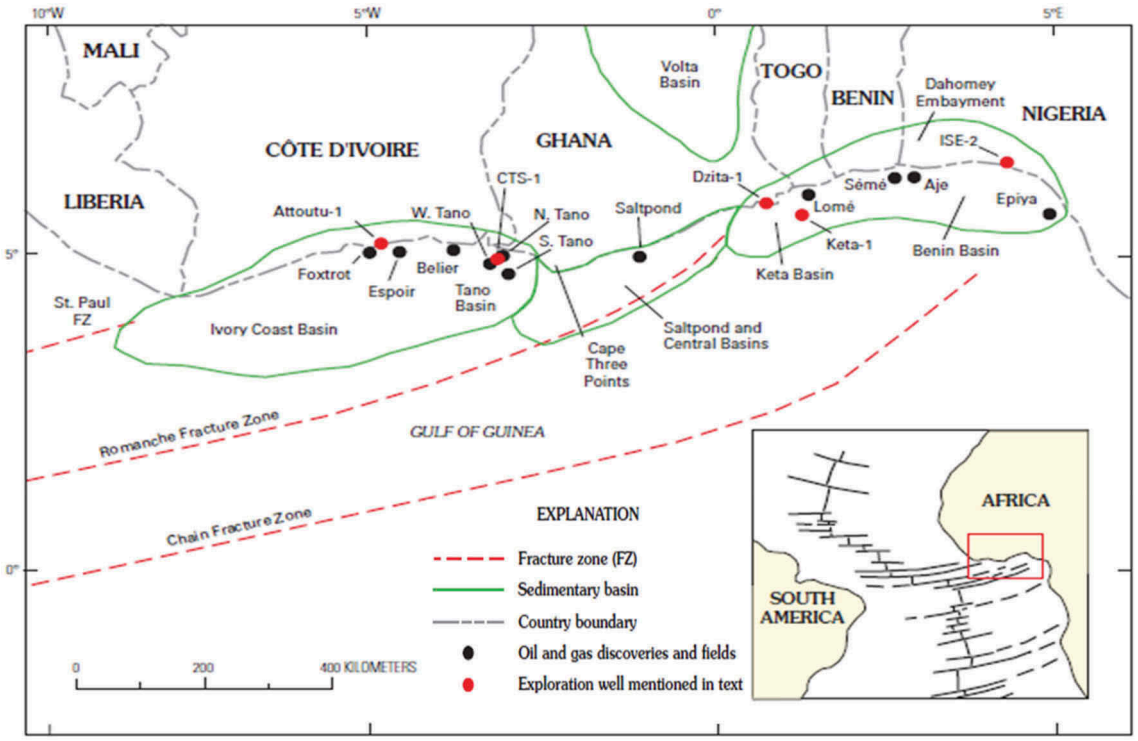

Figure 2. Major features of the Gulf of Guinea province, West Africa (After Kjemperud et al. 1992).

1992). This province is structurally divided by three major transform fault zones, the St. Paul fracture zone along the northwestern boundary, the Romanche fracture zone that separates Ivory Coast, Central and Saltpond Basins from the Keta Basin and the Chain fracture zone along the eastern boundary. The Keta basin developed as a transform margin along the Romanche Fracture Zone (RFZ) as Africa separated from South America in the Early Cretaceous. The basins continental margin formed at the culmination of Late Jurassic to Early Cretaceous tectonism and was characterised by both block and transform faulting superimposed across an extensive Palaeozoic basin during the break-up of the African, North American and South American paleo-continents (Brownfield and Charpentier 2006).

The Dahomeyan rocks occupy the basement and were formed during the Dahomeyide Orogeny (600 ma ago). The assembly of North-Western Gondwana from

various cratonic fragments postulated to be derived from the break-up of Rodinia supercontinent resulted in Pan-African orogens (Hoffman 1991; Cordani et al. 2003) including the 2000 km long Trans-Saharan orogen (Caby 1987; Trompette 1994) located on the eastern margin of the West African Craton (WAC). The south-eastern segment of the Trans-Saharan belt exposed in southeastern Ghana and adjoining parts of Togo and Benin comprises the Dahomeyide orogen (Affaton, et al. 1991; Castaing et al. 1994; Attoh and Ekwueme 1997). The Dahomeyide orogen of Western Africa is a Pan-African collision belt between the passive continental margin of the West African Craton (WAC) and the Sahara Meta-Craton (SMC) (Caby 1987; Affaton, et al. 1991; Abdelsalam et al. 2002). Rocks of the Dahomeyide are sutured onto the WAC, resulting in nappe stacking and crustal imbrication. In southeastern Ghana, the high pressure (HP) mafic granulites have been referred to as Shai Hills gneiss (Attoh, et al. 1997), and are tectonically juxtaposed with the alkaline gneiss complex in the suture zone. Autochthonous rocks of the deformed edge of the craton are the 2.0 Ga granitoid gneisses known as Ho gneiss.

2. Methods/theory

2.1. 3D Euler Deconvolution

The Euler deconvolution method can be traced back to Hood (1965) who first wrote down Euler's homogeneity equation and derived the structural index that can be defined as a measure of the rate of change with a distance of a field. Thompson (1982) further studied and implemented the method by applying Euler deconvolution to synthetic and real magnetic data along with profiles. In this study, the application of this technique to magnetic data was attempted in other to map relative depth to basement. According to Reid et al. (1990), the 3D form of Euler's equation can be defined as

$$(x-x_0)\frac{\partial T}{\partial x}+(y-y_0)\frac{\partial T}{\partial y}+(z-z_0)\frac{\partial T}{\partial z}=N(B-T) \tag{1}$$

where $\frac{\partial T}{\partial x}$, $\frac{\partial T}{\partial y}$, and $\frac{\partial T}{\partial z}$ are the derivatives of the field in the X, Y, and Z directions, B is the base level of the field and N is the structural index value that needs to be chosen according to a prior knowledge of the source geometry. The source location $(X_o, Y_o \, and \, Z_o)$ and B can be computed by solving a linear system of equations generated from Equation (1). According to Dewangan et al. (2007), the unknown regional field (B) can be approximated using Taylor series as,

$$B(x,y)=B_0+x\frac{dB}{dX}+y\frac{dB}{dY}+O(2) \tag{2}$$

where B_o is the constant background at the centre of a specified window and $O(2)$,represents higher-order terms in the Taylor series expansion. To solve for the source location (X_o, Y_o, Z_o) involves writing Equation (1) in matrix form for each window with "n" data points (Mushayandebvu et al. 2004), thus,

$$\begin{bmatrix} \frac{dT}{dX_1} & \frac{dT}{dY_1} & \frac{dT}{dZ_1} \\ \vdots & \vdots & \vdots \\ \frac{dT}{dX_n} & \frac{dT}{dY_n} & \frac{dT}{dZ_n} \end{bmatrix} \begin{bmatrix} X_0 \\ Y_0 \\ Z_0 \end{bmatrix} = \begin{bmatrix} X_1\frac{dT}{dX_1}+ & Y_1\frac{dT}{dY_1}+ & Z_1\frac{dT}{dZ_1} \\ \vdots & \vdots & \vdots \\ X_n\frac{dT}{dX_n}+ & Y_n\frac{dT}{dY_n}+ & Z_n\frac{dT}{dZ_n} \end{bmatrix} \tag{3}$$

where $\frac{dT}{dX_i}$ represent $\frac{dT}{dX_{x=xi}}$ and similar for the other gradients. Equation (3) is of the form

$$Am=d \tag{4}$$

The least-squares solution of Equation (4) involves solving the normal equation

$$A^TAm=A^Td \tag{5}$$

Thus, multiplying through by the transpose matrix A^T, leading to the solution

$$m=\left(A^TA\right)^{-1}A^Td \tag{6}$$

where $\left(A^TA\right)^{-1}$ is the inverse of $\left(A^TA\right)$ and $\left(A^TA\right)^{-1}A^T$ is called the least square inverse of $'A'$. From Equation (6), the source location (X_o, Y_o, Z_o) can be determined. The application of Euler's method required the generation of an analytic signal grid, finding peaks in the grid using blackely grid peak-picking algorithm, then using the peak locations for located 3D Euler deconvolution. A structural index of 1 with a maximum percentage depth tolerance of 15% was used in this study. This method was preferred because it produces far fewer and reliable solutions than the Standard 3D Euler Deconvolution.

2.2. 2D inverse modelling

The inversion method applied in this study for absolute depth estimation follows Jupp and Vozoff (1975), incorporated into the Potent Software and provide stable iteration for processing geophysical data. 2D inverse modelling was created along with five profiles constructed across strike on gravity bouguer anomaly map using the potent computer program. Iterative or non-linear inversion was applied because it can be used with models that are more geologically realistic. This technique is essentially the same as forward modelling except that an automated routine is used to determine the adjustment to be made to the model parameters. Also, a calculated measurement of fit such as root-mean-square (RMS) is used in place of

an interpreter's visual inspection. The iterative method successively improves a current model until the error measure is small and the parameters are stable with respect to reasonable changes in the model. In formulating the discrete inverse problem, the column vector of "M" number of model parameters is introduced as

$$\vec{m} = \{m_{1,}m_{2,\ldots\ldots,}m_M\}^T \tag{7}$$

where "T" denotes the matrix transpose. Similarly, the "N" number of data measured by geophysical surveys are collected into the data vector

$$\vec{d}_m = \left\{d_1^{(m)}, d_2^{(m)}, \ldots\ldots, d_N^{(m)}\right\}^T \tag{8}$$

Let the calculated theoretical data be sorted into the following N-dimensional vector

$$\vec{d}_c = \left\{d_1^{(c)}, d_2^{(c)}, \ldots\ldots, d_N^{(c)}\right\}^T \tag{9}$$

a connection between vectors $\vec{d}_c$ and is given as,

$$\vec{d}_c = \vec{g}(\vec{m})$$

The forward problem generates a set of model data for each setting of "m" and denoted as a vector function by

$$\mathrm{g(m)}=(g_1(m), g_2(m), \ldots\ldots, g_M(M))^T \tag{10}$$

Here,g_i(m) is the value predicted by the model and corresponds to the observation data $'d_i'$. The inverse problem determines values of "m" such that g(m) matches "d" in some sense. Using the familiar Root Mean Squared (RMS), the relative error between model and data is estimated by

$$\mathrm{F(X)}=\left\{\frac{1}{M}\sum_{i=1}^{M}\frac{(d_i-g_i)^2}{{d_i}^2}\right\}^{\frac{1}{2}} \tag{11}$$

We derived the partial derivatives of the model data by expanding g(m) about "M" in a Taylor series expansion as

$$\mathrm{g(m}+\delta\mathrm{M)}=(g(m)+G+R(g,\delta\mathrm{M}) \tag{12}$$

where "G" is the Jacobian matrix of the vector function g(m) given by

$$\mathrm{G}=\left|\frac{\partial g_i}{\partial m_j}\right|_{i=1,M} \tag{13}$$

And $R(g,)$ is a remainder term with$R$ given as

$$\|\mathrm{R}\| = 0\left(\|\delta\mathrm{M}\|^2\right) \tag{14}$$

The objective function to be minimised was given by:

$$\mathrm{E}=\|\varepsilon - G\delta\mathrm{M}\|_{W'} \tag{15}$$

where $\varepsilon = d - g$ and W' is a diagonal weighting matrix. By applying the weighted least squares iteratively and setting depth as model parameters, the function "E" is minimised as follows

$$\begin{aligned} E &= \vec{e}^T\vec{e} \\ &= \sum_{k=1}^{N}\left(d_k - \sum_{i=1}^{M} G_{ki}m_i\right) \\ &\quad \sum_{r=1}^{N} W_{kr}\left(d_r - \sum_{j=1}^{M} G_{rj}m_j\right) \end{aligned} \tag{16}$$

where $\frac{\partial E}{\partial m_l} = 0$ and minimise to the normal equation,

$$\begin{aligned} \frac{\partial E}{\partial m_l} &= 2\sum_{i=1}^{M} m_i \sum_{k=1}^{N}\sum_{r=1}^{N} W_{kr}\ G_{ki}\ G_{rl} \\ &\quad - 2\sum_{k=1}^{N} d_k \sum_{k=1}^{N} W_{kr}\ G_{rl} = 0 \end{aligned} \tag{17}$$

With a vectorial form,

$$\underline{\underline{G^T}}\,\underline{\underline{W}}\,\underline{\underline{G}}\,\vec{m} = \underline{\underline{G^T}}\,\underline{\underline{W}}\,\vec{d} \tag{18}$$

Here, the model parameters are estimated from

$$\vec{m} = \left(\underline{\underline{G^T}}\,\underline{\underline{W}}\,\underline{\underline{G}}\right)^{-1}\underline{\underline{G^T}}\,\underline{\underline{W}}\,\vec{d} \tag{19}$$

From the above Equation (19), absolute depth to the basement was calculated with their level of estimation accuracy given by the RMS value.

3. Results and interpretation

3.1. Located 3D Euler Deconvolution

The total magnetic intensity (TMI) map as shown in Figure 3 shows the variations of magnetic intensities across the basin after the various data reduction techniques have been applied to the magnetic data. The magnetic intensities range between −72.607 and 73.003 nT. The anomalies observed are related to significant susceptibility contrast between the highly magnetic basement and the non-magnetic sediments. Figure 4 shows the Total Magnetic Intensity Map Reduced to the Pole (RTP). This filter transformed the anomalies such that they are centred over their subsurface causative bodies with magnetic intensities between −94.534 and 137.783 nT. Most of the anomalies observed are in the northeast-southwest direction and conform with basement structural trends. The Euler plots in (Figure 5) clearly define depth solutions from 500 m to >2500 m. The depths distribution across the entire basin was not uniform. Most of the Euler solutions in the north showed the rather shallower depth of about 500 m to 1500 m (blue to yellow solutions) for the possible causative sources. To the south and east of the study area, the solutions are situated at deeper depths (between 2000 m to greater than 2500 m) with fewer less than 500 m solutions along the edges of the basin. Non-uniform depth distribution from shallow to deeper depths also characterised the central area of the basin.

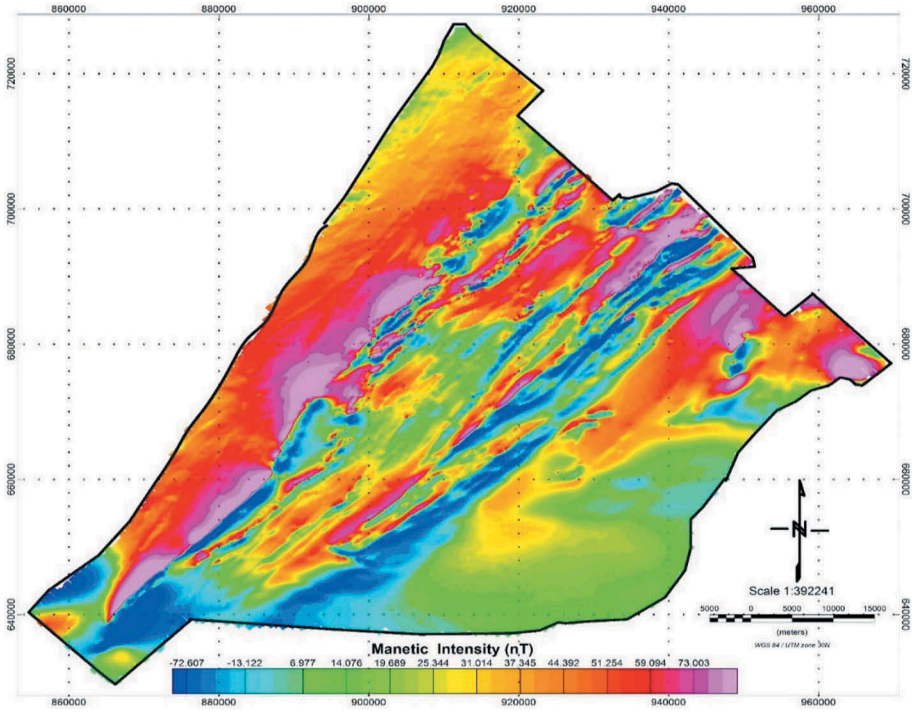

Figure 3. Total Magnetic Intensity (TMI) map of study area.

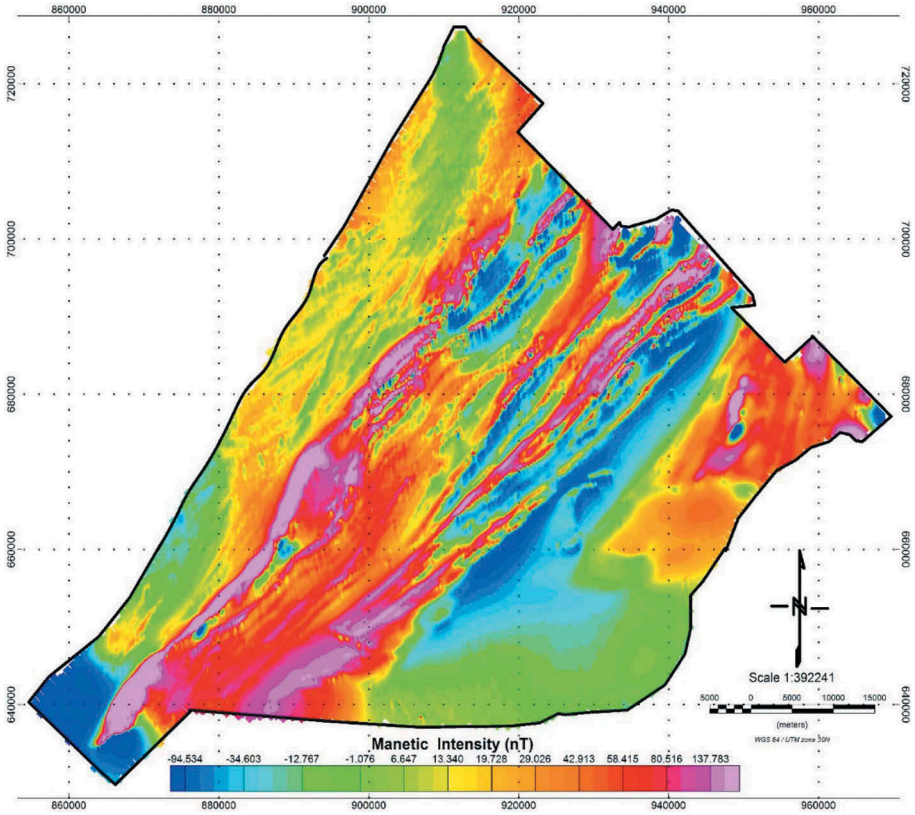

Figure 4. Total Magnetic Intensity grid map reduced to pole.

Figure 6 shows the gridded depth solutions from the Euler deconvolution. As represented on the map, deeper areas (>2000 m) are coloured red/magenta whilst blue, green and yellows represented shallower depths (<2000 m). The black dashes indicate the landward extent of the basin, thus, the boundary between the water and the land. From the map, much deeper depths occur to the south of this boundary whilst shallower depth occupies the north. Cumulatively across the basin, the depth increases from north-to-south as one moves from onshore to offshore. The basin opens southward and portray a conical geometry or shape.

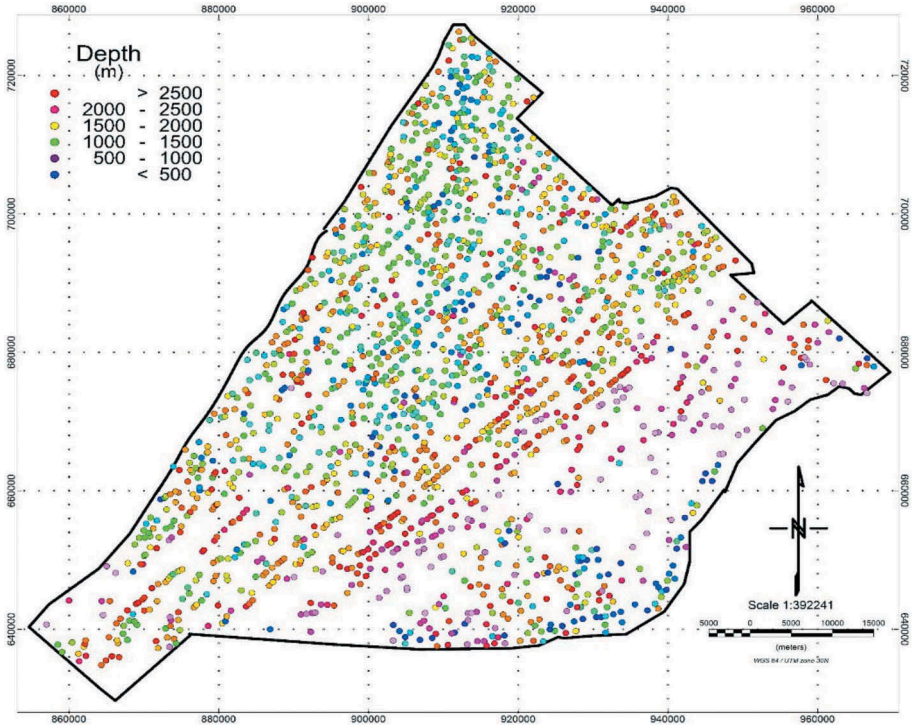

Figure 5. Located Euler Deconvolution map of the study area.

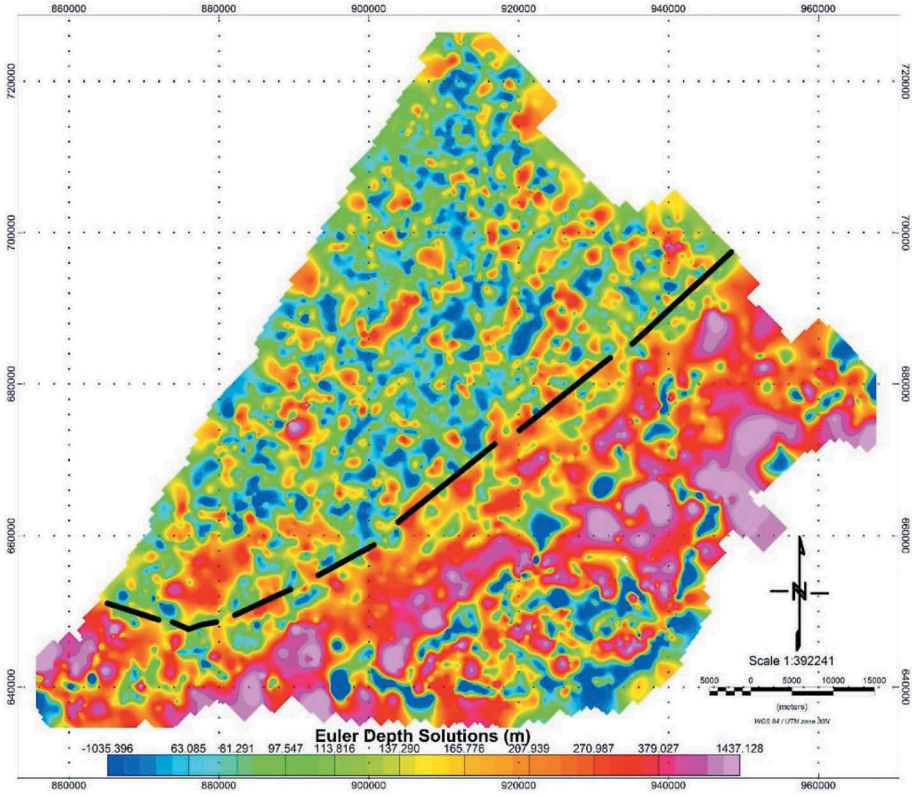

Figure 6. Euler solutions depth grid map.

The Euler deconvolution further provided an idea of the thickness of sedimentary succession overlying the basement at various locations. It can be concluded that much thicker sedimentary succession occurs south and east of the basin as compared to the north. The depth solutions also reveal the spatial relationship between the paleo-topographic highs and lows in the basement. The structural lows are related to deeper depth solutions areas (south and east) which represents basement syncline/troughs whilst the structural highs were shown by shallower depth solutions areas (north) and indicate basement anticlines/uplift.

3.2. 2D gravity inverse modelling

Five profiles were created on the Bouguer gravity anomaly map (Figure 7) namely A1-B1, A2-B2, A3-B3, A4-B4 and A5-B5 across gravity anomalies S1, S2 and S7. These profiles were imported into the potent software which first provided an avenue to forward model the profile data. Using appropriate source bodies for modelling, the calculated gravity was changed to fit the observed gravity at various points. The model was then inverted using an automated means provided by the software. Various parameters such as the depth, width, density and geometry of the source body were automatically calculated from the created model (Table 1).

Figure 8 shows the plan view of the created models. Almost all the models showed a significant level of fit between the observed (red) and calculated (blues) anomalies with their misfit estimated by the Root Mean Square Difference (RMS) values. The basement was modelled with a cylinder from a prior knowledge of a possible volcanic intrusion at it central part shown by the high anomalies S1 and S2. Model 1, produced from anomaly S1 (profile A1-B1), South-east of the basin estimated the depth to the magnetic basement as 1.936 km whilst model 3 (produced from anomaly S2, profile A3-B3) gave a depth of 2.496 km for the Central part with a Root Mean Square Difference (RMS DIFF) of 1.2% and 0.9%, respectively. An absolute depth of 2.487 km was given for the northern area by model 4 (from profile A4-B4). Both model 3 and 4 were produced from the same anomaly, hence their similar depth values. The highest depth estimate was 3.573 km which occurs south of the study area (anomaly S7, profile A5-B5).

Table 1. Estimated modelled parameters.

Modelled parameter	Model 1	Model 3	Model 4	Model 5
Density diff. (g/cm^3)	1.012	0.975	0.912	0.314
Depth (km)	**1.936**	**2.496**	**2.487**	**3.573**
Width (m)	2,356	3,845	3,465	10,783
Strike (^{0})	85.8	46.7	46.3	104.2
Azimuth (^{0})	175.9	136.7	134.0	178.3
DIP (^{0})	89	81	84	88
RMS DIFF.	0.9%	0.7%	1.2%	1.2%

4. Conclusion

Structural trends in the basin is mostly in the north-east-southwest direction as indicated by observed anomalies patterns. The applied methods showed similar depth estimate across the basin, although the 3D Euler Deconvolution estimated relative depth as compared to absolute depth by the 2D Inverse modelling. Both methods estimated higher depth to the south and east of the basin compared to shallower depths to the north of the basin. Depth to magnetic basement across the basin was not uniform as shown by the Euler depth solutions. Deeper depths occur to the south and east (>2000 m) while shallower depths occur to the north (<2000 m). It can further be concluded that much thicker sedimentary succession occupies south and east of the basin as compared to

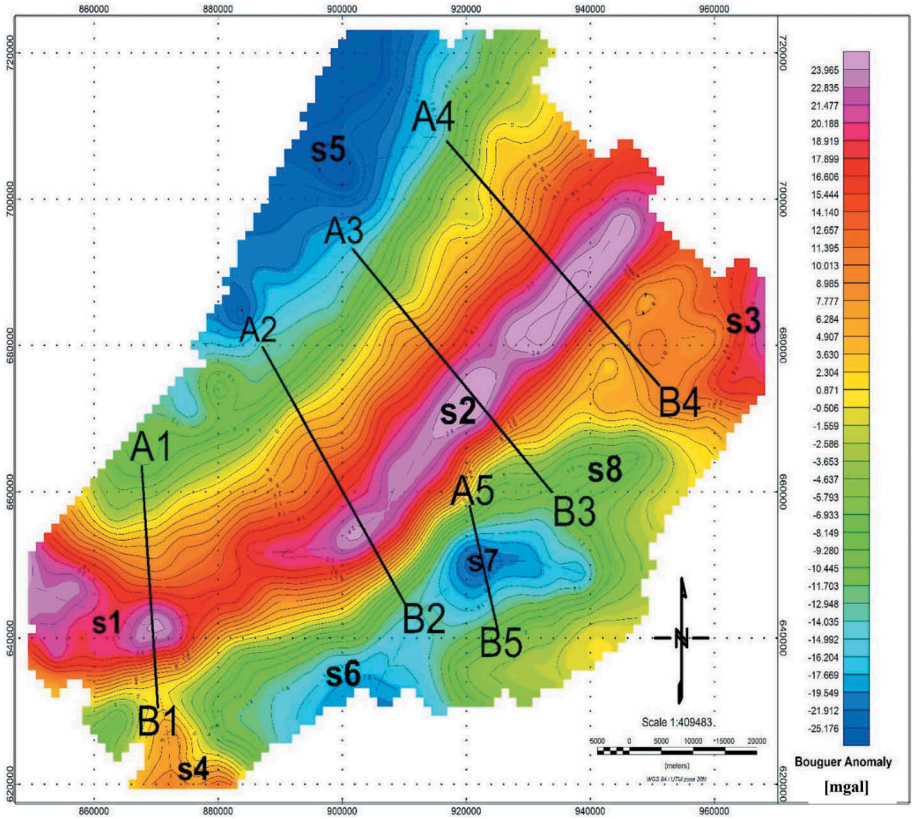

Figure 7. Bouguer gravity anomaly map of the study area.

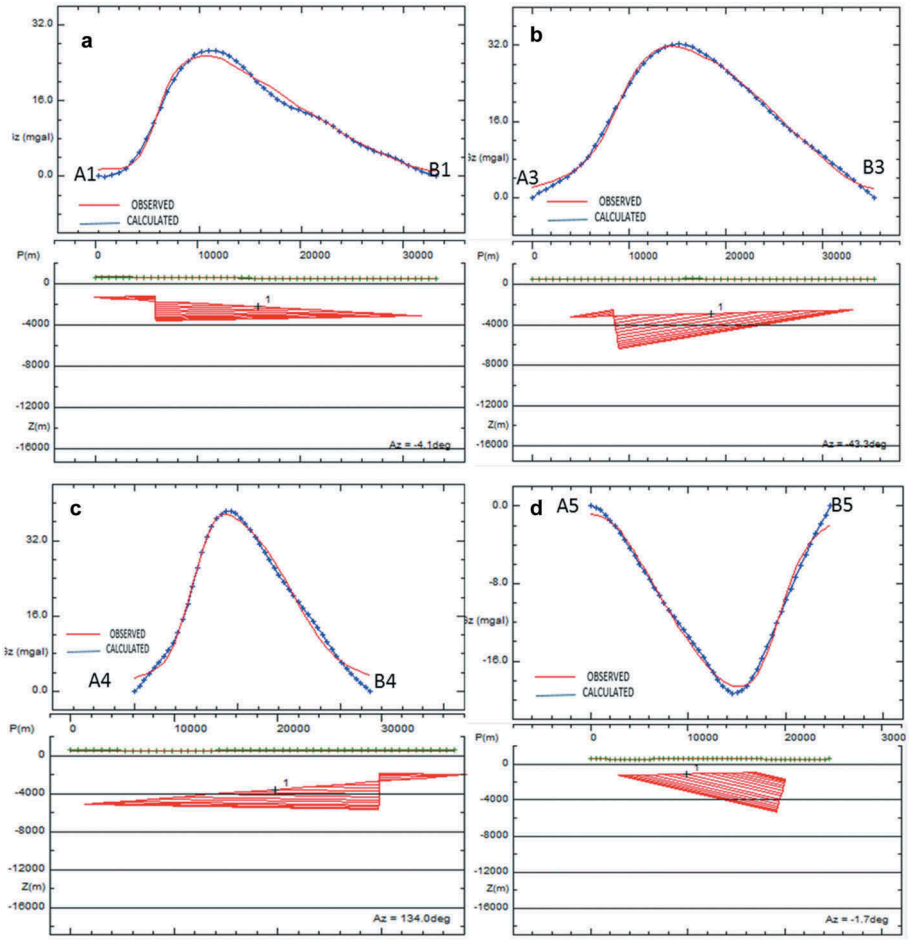

Figure 8. 2D gravity models (a) Model 1, produced from profile A1-B1, (b) Model 3, produced from profile A3-B3, (c) Model 4, produced from profile A4-B4, (d) Model 5, produced from profile A5-B5.

the north. The highest depth estimated was 3.573 km which occurred further south of the basin. In terms of geometry, the basin is conical shaped and southward sloping. The applied methods were effective in evaluating depth to basement and their application enhances initial decision-making in exploration.

Acknowledgements

The described article was carried out as part of the EFOP-3.6.1-16-2016-00011 "Younger and Renewing University – Innovative Knowledge City – institutional development of the University of Miskolc aiming at intelligent specialization" project implemented in the framework of the Szechenyi 2020 program. The realization of this project is supported by the European Union, co-financed by the European Social Fund.

Disclosure statement

No potential conflict of interest was reported by the authors.

References

Abdelsalam MG, Liégeois JP, Stern RJ. 2002. The Saharan Metacraton. J Afr Earth Sci. 34(3–4):119–136. doi:10.1016/S0899-5362(02)00013-1.

Affaton P, Rahaman MA, Trompette, R, Sougy, J, 1991. The Dahomeyide Orogen: tectonothermal evolution and relationships with the Volta Basin. In *The West African orogens and circum-Atlantic correlatives* (pp. 107–122). Springer, Berlin, Heidelberg.

Akpati BN. 1975. Source and dispersal of Holocene sediments on the continental shelf of ghana. *West Africa: UNESCO SCI RP600*, 874:43.

Atta-Peters D, Anan-Yorke, Anani C. 2012. Devonian miospores from atiavi-1 well in the keta basin, southeastern ghana. *Research Journal of Environmental and Earth Sciences*. 4(12):1052–1059.

Attoh K, Ekwueme BN. 1997. In: de Wit MJ, Ashwall L, editors. The West African shield. Oxford University Press, *Greenstonebelts*; p. 513–524. Oxford University Press, Oxford, England, UK.

Attoh K, Dallmeyer RD, Affaton P. 1997. Chronology of Nappe assembly in the Pan-African Dahomeyide Orogen, West Africa: evidence from 40ar/39ar mineral ages. Precambrian Res. 82(1–2):153–171. doi:10.1016/S0301-9268(96)00031-9.

Brownfield ME, Charpentier RR. 2006. Geology and total petroleum systems of the Gulf of Guinea province of West Africa. U.S Geol Surv Bull. 2207-C:32.

Caby R. 1987. The Pan-African belt of West Africa from the Saharan desert to the Gulf of Benin. *Anatomy of Mountain Ranges*, 1, pp.129–170. Princeton University Press, Princeton, New Jersey.

Castaing C, Feybesse JL, Thieblemont D, Triboulet C, Chevremont P. 1994. Palaeogeographical reconstructions of the Pan, African/brasiliano orogen: closure of an

oceanic domain or intracontinental convergence between major blocks? Precambrian Res. 67(1–4):327–344. doi:10.1016/0301-9268(94)90095-7.

Clifford AC. 1986. African oil—past, present, and future. In Halbouty MT, Editor., Future Petroleum Provinces of the World, Proceedings of The Wallace E. Pratt Memorial Conference. Vol. 40. December 1984; Phoenix: American Association of Petroleum Geologists Memoir; p. 339–372.

Cordani UG, D'Agrella MS, Brito-Neves BD, Trindade RIF. 2003. Tearing up Rodinia: the Neoproterozoic paleogeography of South American Cratonic Fragments. Terra Nova. 15 (5):350–359. doi:10.1046/j.1365-3121.2003.00506.x.

Dewangan P, Ramprasad T, Ramana MV, Desa M, Shailaja B. 2007. Automatic interpretation of magnetic data using Euler Deconvolution with nonlinear background. Pure Appl Geophys. 164(11):2359–2372. doi:10.1007/s00024-007-0264-x.

Hoffman PF. 1991. Did the breakout of Laurentia turn Gondwanaland inside-out? Science. 252(5011):5011. doi:10.1126/science.252.5011.1409.

Hood P. 1965. Gradient measurements in aeromagnetic surveying. Geophysics. 30(5):891–902. doi:10.1190/1.1439666.

Jupp DLB, Vozoff K. 1975. Stable iterative methods for the inversion of geophysical data. Geophys J.R Astr Soc. 42(3):957–976. doi:10.1111/j.1365-246X.1975.tb06461.x.

Kjemperud A, Agbesinyale W. and Agdestein T, Gustafsson, Yükler A,. 1992. Tectono-stratigraphic history of the Keta Basin, Ghana with emphasis on late erosional episodes. *Geol. Afr.: Coll. Geol. Libreville, Rec. Communic*, pp.55–69.

Mushayandebvu MF, Lesurz V, Reid AB, Fairhead JD. 2004. Grid Euler Deconvolution with constraints for 2D structures. Geophysics. 69:489–496. doi:10.1190/1.1707069.

Reid AB, Allsop JM, Granser H, Millett AJ, Somerton IW. 1990. Magnetic interpretation in three dimensions using Euler Deconvolution. Geophysics. 55:80–91. doi:10.1190/1.1442774.

Thompson DT. 1982. Euldph: A new technique for making computer-assisted depth estimates from magnetic data. Geophysics. 47(1):31–37. doi:10.1190/1.1441278.

Trompette R. 1994. *Geology of western Gondwana (2000-500 Ma): Pan-Africa-Brasiliano aggregation of South America and Africa* (No. 55 (215-13) TRO).